Accepted Manuscript

Biosynthesized Co-doped TiO_2 nanoparticles based anode for lithium-ion battery application and investigating the influence of dopant concentrations on its performance

Anil A. Kashale, Akash S. Rasal, Gokul P. Kamble, Vijay H. Ingole, Pravin K. Dwivedi, Swapnil J. Rajoba, Lata D. Jadhav, Yong-Chien Ling, Jia-Yaw Chang, Anil V. Ghule

PII: S1359-8368(18)32042-0

DOI: https://doi.org/10.1016/j.compositesb.2018.12.001

Reference: JCOMB 6330

To appear in: *Composites Part B*

Received Date: 30 June 2018

Revised Date: 21 September 2018

Accepted Date: 2 December 2018

Please cite this article as: Kashale AA, Rasal AS, Kamble GP, Ingole VH, Dwivedi PK, Rajoba SJ, Jadhav LD, Ling Y-C, Chang J-Y, Ghule AV, Biosynthesized Co-doped TiO_2 nanoparticles based anode for lithium-ion battery application and investigating the influence of dopant concentrations on its performance, *Composites Part B* (2019), doi: https://doi.org/10.1016/j.compositesb.2018.12.001.

Biosynthesized Co-Doped TiO_2 Nanoparticles based Anode for Lithium-Ion Battery Application and Investigating the Influence of Dopant Concentrations on its Performance

Anil A. Kashale[a,b,g], Akash S. Rasal[g], Gokul P. Kamble[g], Vijay H. Ingole[a,g], Pravin K. Dwivedi[c], Swapnil J. Rajoba[d], Lata D. Jadhav[d], Yong-Chien Ling[e], Jia-Yaw Chang*[f] and Anil V. Ghule*[a,e,g]

[a]*Department of Nanotechnology, Dr. Babasaheb Ambedkar Marathwada University, Aurangabad 431004, Maharashtra, India.*

[b]*Department of Chemistry, Dr. Babasaheb Ambedkar Marathwada University, Aurangabad 431004, Maharashtra, India*

[c]*Physical and Materials Chemistry Division, CSIR-National Chemical Laboratory (CSIR-NCL) Pune 411008, Maharashtra, India*

[d]*Electrochemical Energy Materials Laboratory, Department of Physics, Rajaram College, Kolhapur 416004, Maharashtra, India*

[e]*Department of Chemistry, National Tsing Hua University, Hsinchu 30013, Taiwan*

[f]*Department of Chemical Engineering, National Taiwan University of Science and Technology, Taipei 10607, Taiwan, Email: jychang@mail.nthust.edu.tw*

[g]*Department of Chemistry, Shivaji University, Kolhapur 416004, Maharashtra, India*

Email: anighule@gmail.com, avg_chem@unishivaji.ac.in

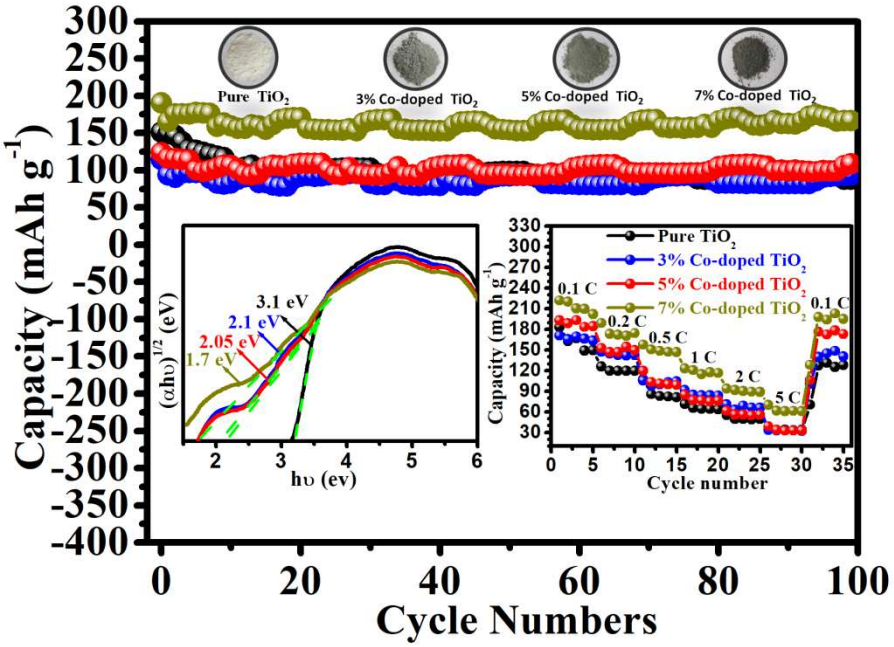

Biosynthesized Co-Doped TiO_2 Nanoparticles based Anode for Lithium-Ion Battery Application and Investigating the Influence of Dopant Concentrations on its Performance

Anil A. Kashale[a,b,g], Akash S. Rasal[g], Gokul P. Kamble[g], Vijay H. Ingole[a,g], Pravin K. Dwivedi[c], Swapnil J. Rajoba[d], Lata D. Jadhav[d], Yong-Chien Ling[e], Jia-Yaw Chang*[f] and Anil V. Ghule*[a,e,g]

[a]*Department of Nanotechnology, Dr. Babasaheb Ambedkar Marathwada University, Aurangabad 431004, Maharashtra, India*

[b]*Department of Chemistry, Dr. Babasaheb Ambedkar Marathwada University, Aurangabad 431004, Maharashtra, India*

[c]*Physical and Materials Chemistry Division, CSIR-National Chemical Laboratory (CSIR-NCL) Pune 411008, Maharashtra, India*

[d]*Electrochemical Energy Materials Laboratory, Department of Physics, Rajaram College, Kolhapur 416004, Maharashtra, India*

[e]*Department of Chemistry, National Tsing Hua University, Hsinchu 30013, Taiwan*

[f]*Department of Chemical Engineering, National Taiwan University of Science and Technology, Taipei 10607, Taiwan, Email: jychang@mail.nthust.edu.tw*

[g]*Department of Chemistry, Shivaji University, Kolhapur 416004, Maharashtra, India*

Email: anighule@gmail.com, avg_chem@unishivaji.ac.in

Corresponding authors:

Anil Vithal Ghule (anighule@gmail.com; avg_chem@unishivaji.ac.in)

Jia-Yaw Chang (jychang@mail.nthust.edu.tw)

Abstract

TiO_2 is a good alternative anode material for lithium-ion battery application because of its incomparable high structural stability and safety during the charge/discharge cycles. However, the low intrinsic conductivity of TiO_2 has been a limiting factor affecting its cycling and rate capability performance. Here in this work, we present Co-doped TiO_2 nanoparticles based anode with good reversibility, cycling stability and rate capability performance for its envisaged application in lithium-ion battery. The Co-doped TiO_2 nanoparticles with different Co concentrations (3%, 5%, and 7%) are synthesized using simple and economic biomediated green approach, wherein $TiCl_4$ and Co precursors are allowed to react in Bengal gram bean extract containing biomolecules which act as natural capping agents to control the size of nanoparticles. Among the pure TiO_2 and different Co-doped TiO_2 samples, the 7% Co-doped TiO_2 anode show the highest capacity of 167 mAh g^{-1} (88.3%) after 100 cycles at the 0.5C current density. The Co-doped TiO_2 shows higher and stable coulombic efficiency up to 100 GCD cycles indicating good reversibility. Based on the results, it is expected that the Co-doped TiO_2 nanoparticles might be contributing to the enhanced electronic conductivity providing an efficient pathway for fast electron transfer.

Keywords: Biomediated; Green; Co-doped TiO_2 Composite; Anode; Co doping effect; Lithium Ion Batteries

Introduction

Titanium dioxide (TiO_2) is considered as the workhorse of technological development because of its unique physicochemical properties leading to versatile applications in energy-related devices, energy harvesting systems, water-splitting devices, dye-sensitized solar cells, energy storage, photocatalysts etc [1-8]. Apart from these applications, researchers have used TiO_2 as an anode material in lithium ion batteries due to its low cost, easy availability, non-toxicity, high abundance, excellent structural stability with lithium, long cycle life, high capacity and very low volume change during lithium ion intercalation/deintercalation (~4%) [9-13]. Besides this TiO_2 exhibits high operating voltage (>1.5 V *Vs* Li) during lithium ion intercalation/deintercalation process, which is obviously higher than the operating voltage of graphite anodes, thereby avoiding the formation of SEI (Solid Electrolyte Interphase) and dendrite of lithium [14]. These characteristics make it a promising anode material for heavy-duty, long-life and large-scale energy storage batteries [15-17]. However, poor reversible capacity, the poor cycling performance, poor rate capability, relatively less electron (due to wide band gap) and ionic conductivity has hampered its use as electrode material in LIBs [18-20].

Extensive work and several attempts have been made by the researchers by developing different strategies to overcome the above drawback of TiO_2 by designing TiO_2-based composites with carbon conducting materials (Graphene, CNTs etc.) [21-24]. However, introducing the large quantity of carbon (conducting agents) in the composite reduces the capacity of electrode material owing to the formation of the dead layer with increasing concentration of carbon (conducting agents). Thus, there is need to find other alternative approaches to improve the electron mobility and rate capability of TiO_2 materials. Recent literature reports have revealed that metal doping exhibits considerable advantage to alter the intrinsic conductivity and rate capability of TiO_2, consequently due to the generation of

oxygen vacancies and decrease in the band gap of TiO_2 thereby improving Li-ion storage properties [25-30]. It is reported that the doping of cobalt ion can improve the electronic conductivity of metal oxides. H. Kong et al. [31] synthesized the Co-doped Fe_2O_3 which exhibited significantly enhanced electrochemical performance with excellent rate capability and high reversible capacity when compared to pure Fe_2O_3. C. Zhang et al. [32] synthesized the Co-doped $Li_4Ti_5O_{12}$ showing better electrochemical performance compared to pure $Li_4Ti_5O_{12}$. The results indicate that the Co-doping leads to the generation of "O" vacancies which enhances Li intercalation in $Li_4Ti_5O_{12}$ materials. Interestingly, Thi T. et al. [33] reported the synthesis of Co-doped NiO nanoparticles which resulted in increased concentration of hole contributing to the improved conductivity of NiO. W. Zhang et al.[34] synthesized the Mn-doped TiO_2 nanosheets demonstrating superior reversible capacity, rate capability, and improved cycling stability. The observed results were ascribed to the roles of Mn ions in inhibiting crystal structure conversion under calcination and improving the electrode-electrolyte interface stability. Qun Li et al. [35] synthesized Cu doped manganese oxide nanoparticles showing significant improvement in electronic conductivity and lithium diffusivity in the electrode. Based on the literature survey, it is observed that the metal doping plays an important role and can improve the reversible capacity, cycle performance, and rate capability of transition metal oxides (TMOs) by enhancing electronic conductivity. However, to the best of our knowledge, only one report on Co-doped TiO_2 [36] materials for sodium ion battery application exist, which clearly shows the improved electrochemical performance of Co-doped TiO_2 electrode when compared to pure TiO_2. The observed enhancement in electronic conductivity of Co-doped TiO_2 in respect to pure TiO_2 is attributed to Co doping. With this motivation, in the present work, we have synthesized the Co-doped TiO_2 nanoparticles by using simple biomediated green approach, wherein Ti and Co precursors are

allowed to react in Bengal gram bean extract containing biomolecules which act as natural capping agents to control the size of nanoparticles.

In the typical process in this work, Co-doped TiO_2 nanoparticles have been synthesized by a facile, cost-effective, scalable and eco-friendly approach using remnant water (ideally kitchen waste) collected from soaked Bengal gram beans (*Cicer arietinum L.*). The gram bean extract containing pectin biomolecules are responsible for the synthesis of Co-doped TiO_2 nanoparticles. Pectin is a complex polysaccharide, that is present in most primary cell walls and it acts as a capping agent and hinders the aggregation [13]. Interesting, when Co-doped TiO_2 nanoparticles based thin film is used as an anode material for LIBs, it demonstrates the high capacity and excellent rate capability compared to pure TiO_2 and this improvement can be due to the decrease in the band gap, which helps to enhance the electronic conductivity of TiO_2. The results indicate that Co-doped TiO_2 is a promising anode material for high-performance LIBs.

2 Experimental

2.1 Chemicals

Titanium chloride ($TiCl_4$), cobalt (II) chloride dihydrate ($CoCl_2.2H_2O$) and ammonia (AR grade 28 %) purchased from Merck were used as such without further purification for the synthesis of Co-doped TiO_2 nanoparticles. Bengal gram beans (*Cicer arietinum L.*) were obtained from a local market in Aurangabad, India.

2.2 Synthesis of Gram Bean Extract

20 g of dry Bengal gram beans (*Cicer arietinum* L.) were soaked in 100 mL of DI water for 6 h at room temperature (25°C). Thereafter, the soaked seeds were removed and the extract was filtrated using a glass-fiber filter (GF/F) to be free from particulate matter. The filtered solution i.e. the gram bean extract (remnant water) is used for the synthesis of Co-doped TiO_2 nanoparticles.

2.3 Synthesis of Cobalt Doped TiO_2 Nanoparticles

For the typical synthesis of 3 wt %, 5 wt %, and 7 wt % Co-doped TiO_2 nanoparticles using biosynthesis method, 10 mL of gram bean extract was taken in three beakers which were first diluted to 50 mL. Further, 6.9 mL of $TiCl_4$ solution was dropped wise added in each beaker containing 50 mL diluted gram bean extract. Cobalt chloride was used as a source of cobalt and an appropriate amount of $CoCl_2.2H_2O$ was added to this solution for having 3 wt%, 5 wt %, and 7 wt % Co doping, respectively. Subsequently, the pH of the solution was adjusted to 7 using ammonia solution and formation of titanium-hydroxide pectin gel, which shrinks and inhibits the further growth of the nanoparticles. The shrunk gel was washed with deionized water. The powder was dried in an electric oven at 100 °C and subsequently calcined at 400 °C for 3 h to remove the organic the contaminants. Pristine TiO_2 was also prepared in the same way without doping cobalt ion for better comparison. All Co-doped TiO_2 and pure TiO_2 nanoparticles so produced were characterized for their preliminary structural and morphological properties.

2.4 Material Characterization

Powder X-ray diffraction measurement was carried out using Bruker AXS D8 Advance X-ray diffractometer equipped with Cu $K\alpha_1$ radiation between 10° and 80°. Raman spectra were carried out using a UniG2D Raman Spectroscope (UniNano Tech) with a 532 nm CW laser as the light source. UV-visible Diffuse Reflectance spectra (UV-Vis DRS) of the samples were recorded using UV-Vis spectrophotometer (LabIndia, UV 3092). Morphology of the as-synthesized cobalt-doped TiO_2 materials and calcined pure TiO_2 were investigated using scanning electron microscopy (SEM) measurement on a JSM 6500F microscope (JEOL) operating at 15 kV. Particle size and morphology of 5 wt % Co-doped TiO_2 and pure TiO_2 were recorded using transmission electron microscopy (TEM) measurement on an FEI Tecnai G2 F20 microscope (Philips) with a field-emission gun operating at a 200 kV. Specimens

were prepared by ultrasonication of TiO_2 nanoparticles in ethanol followed by dropping the suspension on a carbon-coated copper grid.

2.5 Electrode and Coin Cell Preparation for Electrochemical

The electrodes for the electrochemical analysis were prepared by coating a composite slurry of 80 wt % of active materials (Co-doped TiO_2), 15 wt % of conducting carbon (super-P, timcal) and 5 wt % of poly(vinylidene difluoride) (PVDF) binder prepared in N-methyl-2-pyrrolidone (NMP) on a carbon-coated copper foil by using doctor blade method, wherein, the copper foil act as a current collector. This composite coated foil was then subsequently dried at 60 °C for 24 h and then cut into a circular disk with the help of a punching machine fitted with cutters suitable for coin cells of CR2032. The material loadings in the range of 2.0-4.0 mg were achieved. The CR2032 cells for electrochemical testing were assembled inside an argon-filled glove box at an extremely low oxygen level of less than 0.1 ppm. The metallic lithium (Li) disc was used as both counter and reference electrode on the other side. The two electrodes were separated by a Whatman Glass microfiber filter separator soaked in the electrolyte solution. 1 M Lithium Hexafluorophosphate ($LiPF_6$) in 1:1 volume ratio of ethylene carbonate (EC) and dimethyl carbonate (DMC) mixture was used as the electrolyte. Cyclic voltammetry (at scan rate 0.2 mV s^{-1}) and galvanostatic cycling profile (at a constant current density of 0.1 C) measurements were carried out using Biologic-108 battery cycler in the potential window 0.01 to 3 V for half-cell configurations at ambient temperature conditions.

3. Result and Discussion

3.1. X-ray diffraction (XRD) pattern

The crystal phase composition of synthesized pure and Co-doped TiO_2 nanoparticles is investigated by using XRD pattern as shown in **Figure 1**. The XRD pattern of pure and Co-doped TiO_2 is composed of anatase (JCPDS, No. 02-0387) rather than rutile or brookite

phases. In **Figure 1**, pure TiO_2 reveals high crystallinity showing intense peaks at 2θ values of 25.09°, 37.65°, 47.86°, 53.81°, 54.88°, 62.42°, 68.53°, 70.00°, and 74.93°, which could be indexed to (101), (004), (200), (105), (211), (204), (116), (220) and (215) planes of anatase titania, respectively. The same peak pattern is also observed in the 3% Co, 5% Co and 7% Co-doped TiO_2 nanoparticles. No extra peaks are observed in doped samples (3% Co and 5% Co-doped TiO_2) except for the sample of 7% Co-doped TiO_2 nanoparticles. In this case, additional diffraction peaks observed at 2θ = 31°, 65°, and 72° are attributed to Co_3O_4 and are in good agreement with JCPDS Card No. 80-1536 [37, 38]. The Co_3O_4 peaks are marked as "Co" in the spectra for clarity of presentation. It means that at low concentration (3% Co and 5% Co), the cobalt ions are uniformly dispersed on the host TiO_2 and in case of high concentration (7% Co) a small amount of cobalt oxides particles may be formed on the surface or within the matrix of TiO_2 which is commonly observed at high concentration of metal doping. Furthermore, it is clearly observed in **Figure 1** that the intensity of peaks of cobalt doped TiO_2 samples decreases compared to pure TiO_2 and the intensity is found to decrease with increasing cobalt dopant concentration. This is might be due to the formation of oxygen vacancies and decreasing the crystallite size of cobalt doped TiO_2 nanoparticles. The crystallite size of all the samples were calculated with reference to (110) intense peak at 2θ = 25.09 by using the Debye Scherrer's formula, $D=0.9\lambda/\beta\cos\theta$, where D is the crystallite size, λ is the wavelength of X-ray used, and θ is the Bragg angle of diffraction peaks. The crystallite size for pure TiO_2 was found to be 10.8 nm and for 3% Co-TiO_2, 5% Co-TiO_2 and 7% Co-TiO_2 samples it was found to be 9.2, 8.9 and 8.7 nm, respectively.

3.2. Raman Spectra

Raman spectroscopy is one of the important and efficient analysis techniques to confirm the phase and structural changes in TiO_2. **Figure 2** shows the Raman spectra of pure TiO_2 and Co-doped TiO_2 nanoparticles. All samples reflect the six Raman active modes (A_{1g} +

$2B_{1g} + 3_{Eg}$), which denotes that the anatase phase of TiO_2 is predominant [39]. No extra modes are observed except for the sample with 7% Co-doped TiO_2 nanoparticles. The 7% Co-doped TiO_2 nanoparticles show two extra peaks at (E_g) 480 cm^{-1} and (A_{1g}) 687 cm^{-1}, which is attributed to Co_3O_4 [40]. From these results, it is observed that at low concentration (3% Co-doped TiO_2 and 5% Co-doped TiO_2), the cobalt ions are incorporated in the TiO_2 crystalline lattices, but at high concentration (7% Co-doped TiO_2) some cobalt oxides nanoparticles are grown outside the TiO_2 lattices. Furthermore, the intensity of modes decreases with increasing Co-dopant concentration and also shows Raman shifts slightly towards the higher wavenumber (**inset Figure 2**). The observed shift is attributed to the formation of oxygen vacancies and the decrease in the size of TiO_2 nanoparticles with increasing dopants concentration. These results are in good agreement with the XRD results.

3.3. UV-Vis diffuse reflectance spectra (UV-vis DRS) analysis

UV-Vis DRS analysis technique is usually used for determination of energy band gap of powdered or opaque samples. Here we have studied the effect of doping on the band gap of TiO_2 nanoparticles. **Figure 3** shows the UV-vis absorption spectra and energy band gap (**inset in Figure 3**) spectra of pure and Co-doped TiO_2 nanoparticles. The UV-Vis DRS spectrum of pure TiO_2 showed strong absorption edge approximately at 398 nm as commonly observed in anatase TiO_2, while absorption edge of Co-doped TiO_2 (3%, 5% and 7% Co-doped TiO_2) greatly shift into the visible region. Further observation shows that the absorbance in the visible light region (redshift) increases with increasing doping percentage of cobalt. This might be due to intercalation of Co into the lattice of TiO_2 thereby narrowing the band gap [41].

The band gap of all these samples was calculated by using the modified Kubeka Munk equation (1).[42]

$$\alpha(hv) = C_1\left(hv - E_g\right)^2 \qquad (1)$$

$$h\nu = \frac{1240}{\lambda} \qquad (2)$$

Where, α is the optical absorption coefficient, hν is the photon energy, C_1 is the adsorption constant of the indirect transition, λ is the wavelength. The energy band gap values for 0% (pure TiO_2), 3%, 5% and 7% Co-doped TiO_2 corresponding to 3.1, 2.1, 2.05, and 1.7 eV, respectively, were obtained and the results are shown in the inset of **Figure 3**. These results indicate that cobalt doping help to reduce the distance between the conduction band and valence band of TiO_2, which enhances the electronic conductivity of TiO_2.

3.4. Scanning Electron Microscopy (SEM)

The structure and morphology of the biosynthesized pure and Co-doped TiO_2 nanoparticles are also examined by SEM. **Figure 4** shows the micrograph of pure (a) TiO_2, (b) 3%Co-doped TiO_2, (c) 5%Co-doped TiO_2 and (d) 7%Co-doped TiO_2 nanoparticles calcined at 400 °C, which demonstrates the uniform spherical shaped nanoparticles with narrow size distribution. These spherical shaped nanoparticles get agglomerated to form larger particles. No major change in morphology of the Co-doped TiO_2 nanoparticles is observed when compared with pure TiO_2. Furthermore, representative EDX patterns of pure TiO_2 and 5% Co-doped TiO_2 nanoparticles were recorded to investigate the elemental composition. **Figure 5** shows the EDX patterns of pure and 5% Co-doped TiO_2 nanoparticles. The EDX pattern of pure TiO_2 (**Figure 5a**) clearly shows the exclusive presence of Ti and O element confirming the absence of any other impurities in the sample. Similarly, the 5% Co-doped TiO_2 (**Figure 5b**) shows the presence of Co, Ti and O element, which confirms that cobalt is successfully doped in the TiO_2. In Co-doped TiO_2 nanoparticles "Ti" percentage is found to decrease and "O" percentage found to increase as a result of Co doping. This result is in good agreement with the literature report confirming the successful formation of Co-doped TiO_2 nanoparticles.

3.5. Transmission Electron Microscopy (TEM)

TEM is an advanced analysis method to determine the morphology and crystallite size of nanoparticles. With this motivation, we have studied the TEM analysis of pure and 5% Co-doped TiO_2 nanoparticles and the results are shown in **Figure 6**. TEM images of pure and 5% Co-doped TiO_2 nanoparticles clearly show spherically shaped particles with a homogeneous distribution of particle size as shown in **Figure 6a and 6c**. High-resolution TEM images of pure and 5% Co-doped TiO_2 nanoparticles (**Figure 6b and 6d**) show the well-developed fringes, which indicate both nanoparticles are well crystallized. In addition, **Figure 6e and 6f** show the particle size distribution histogram of pure and 5% doped TiO_2. As can be seen from the histogram, the average crystallite size of Co-doped TiO_2 (~9.1 nm) is less than the pure TiO_2 (~11 nm), which is in good agreement with the crystallite size obtained from XRD results.

3.6. Electrochemical Properties

Further, we have studied the effect of cobalt doping concentration on the electrochemical performance of Co-doped TiO_2 (3%, 5% and 7% Co-doped TiO_2) nanoparticles in comparison with pure TiO_2 nanoparticles by making half cell of pure TiO_2 and Co-doped TiO_2 (3%, 5% and 7% Co-doped TiO_2) nanoparticles. **Figure 7a** shows the cyclic voltammetry (CV) analysis of pure TiO_2 and Co-doped TiO_2 (3%, 5% and 7% Co-doped TiO_2) nanoparticles in the potential range of 0.01 to 3 V Vs Li/Li^+ at scan rate of 0.2 mV s^{-1}. From **Figure 7a** it is clearly observed that the nature of CV curves of pure and Co-doped TiO_2 are similar showing redox couple peaks at ~1.68 and ~2.17 V Vs Li/Li^+, which correspond to the lithium ion intercalation into and deintercalation from the interstitial sites of TiO_2. The CV curve reveals that the intensity of oxidation peak decrease and a peak shift to a lower voltage with an increase in Co doping concentration. This observation indicates improved wetting and enhanced Li-ion insertion kinetics with an increase in doping concentration of cobalt [43-45]. The maximum lower shift is observed in 7% Co-doped TiO_2,

which means that the Li-ion insertion kinetics is higher in 7% Co-doped TiO_2 as compared to the pure, 3% Co-doped TiO_2 and 5% Co-doped TiO_2. The increase of Li-ion insertion kinetics and wettability of cobalt doped TiO_2 electrode material is due to the decrease in band gap with an increase in Co doping concentration. In other words, the electronic conductivity of TiO_2 increases with Co doping which is also very well reflected in UV-Vis DRS study.

Figure 7b shows the comparative first galvanostatic charge/discharge profile of pure and Co-doped TiO_2 at a constant current density of 0.1C (1C=335 mAh g^{-1} for 1 mol of Lithium) in the voltage range of 0.01 to 3 V vs Li/Li^+. In the **Figure 7b,** it is clearly observed that the pure TiO_2 shows large irreversible capacity 27 mAh g^{-1} (discharge capacity = 183 mAh g^{-1}, charge capacity 156 mAh g^{-1}). But cobalt-doped TiO_2 shows very low irreversible capacity compared to pure TiO_2. The 3% Co-doped TiO_2, 5% Co-doped TiO_2 and 7% Co-doped TiO_2 shows the 3 mAh g^{-1} (discharge capacity = 160 mAh g^{-1}, charge capacity 157 mAh g^{-1}), 1 mAh g^{-1} (discharge capacity = 188 mAh g^{-1}, charge capacity 187 mAh g^{-1}) and 14 mAh g^{-1} (discharge capacity = 221 mAh g^{-1}, charge capacity 205 mAh g^{-1}) irreversible capacity, respectively. The reduction in irreversible capacity of Co-doped TiO_2 indicates an enhancement in the electrode and electrolyte interaction, decrease in SEI (Solid electrolyte interface) formation and enhanced the electrochemical reversible reaction of TiO_2 nanoparticles. This is attributed to Co-doping which enhances structural stability and also contribute to enhancing the electronic conductivity. The doping of Co introduces the lattice distortion and oxygen vacancies in the TiO_2 lattices due to the difference in the oxidation state of cobalt (Co^{+2}) and titanium (Ti^{+4}) or charge compensation effect, which helps to reduce the bandgap and increase the rate of electron transport [46, 47]. The 7% Co-doped TiO_2 shows the highest discharge capacity (discharge capacity = 221 mAh g^{-1}) when compared to 3% Co-doped TiO_2, 5% Co-doped TiO_2 and pure TiO_2 nanoparticles. This

enhancement might be due to the formation of CO_3O_4 (clearly observed in the XRD and Raman spectra) and TiO_2 composite or synergetic effect of Co_3O_4 and TiO_2 [48].

The stability of synthesized pure TiO_2 and Co-doped TiO_2 are investigated up to the 100 cycles in the potential window range of 0.01 - 3 V vs Li/Li^+ at a constant current density of 0.5 C and the results are shown in **Figure 7c**. Although, the cycling stability, as well as the specific capacity of 7% Co-doped TiO_2 nanoparticles, is high as compared to other three TiO_2 nanoparticles (pure TiO_2, 3% Co-doped TiO_2 and 5% Co-doped TiO_2). The initial specific capacity values for pure TiO_2, 3% Co-doped TiO_2, 5% Co-doped TiO_2 and 7% Co-doped TiO_2 correspond to the 151 mAh g^{-1}, 123 mAh g^{-1}, 114 mAh g^{-1} and 189 mAh g^{-1} respectively. In **Figure 7c** it is clearly observed that the pure TiO_2 gradually shows a decrease in capacity with an increase in cycle number, but in case of Co-doped TiO_2, the specific capacity shows relatively less decrease compared to pure TiO_2. The retention of specific capacity after 100 cycles are 57.6 % (87.6 mAh g^{-1}), 81.5 % (93 mAh g^{-1}), 87.8 % (108 mAh g^{-1}) and 88.3 % (167 mAh g^{-1}) for pure TiO_2, 3% Co-doped TiO_2, 5% Co-doped TiO_2 and 7% Co-doped TiO_2, respectively. Furthermore, the coulombic efficiency graph is shown in Figure 7c, in which it is clearly observed that the initial few cycles in pure TiO_2 show lower coulombic efficiency. However, in the case of cobalt-doped TiO_2 it shows comparatively high coulombic efficiency and it is stable up to 100 GCD cycles. In general, the Co-doped TiO_2 samples show the high retention capacity and coulombic efficiency compared to the pure TiO_2 even after 100 cycles.

Figure 7d shows the results of the investigation of the rate performance of pure and Co-doped TiO_2 nanoparticles at different C-rates (from 0.1 to 5 C). From the rate performance study, it is clearly observed that there is a gradual decrease in specific capacity during first five initial cycles of all electrodes of TiO_2 at 0.1 C, this may be due to the loss of symmetry during phase transition accompanied by a decrease in the unit cell along the c-axis.

Furthermore, the subsequent increase of unit cell volume (~4%) along the b direction results in capacity fading [13, 49-51]. For the further C-rates (0.2 - 5C), the specific capacitance of all electrode of TiO_2 is stable. Among the all the TiO_2 and Co-doped TiO_2 nanoparticles, the 7 % Co-doped TiO_2 nanoparticles show better rate performance as well as high specific capacitance compared with the pure TiO_2, 3% Co-doped TiO_2 and 5% Co-doped TiO_2 electrode materials. The initial specific capacities of pure-TiO_2, 3% Co-doped TiO_2, 5% Co-doped TiO_2 and 7% Co-doped TiO_2 are about 183, 170, 193, and 221 mAh g^{-1} at scan rate 0.1 C, respectively. For further C-rates (0.2 to 5C), the specific capacitance decreases with increase in current density (C-rate) (**results are shown in Table 1**) and when the current density returns back after 5C to the initial current density (C-rate) of 0.1 C, the specific capacity switches to 131 (71.8%), 148 (87.0%), 177 (91.7%) and 203 (91.8%) mAh g^{-1} for the pure TiO_2, 3% Co-doped TiO_2, 5% Co-doped TiO_2 and 7% Co-doped TiO_2, respectively. From the above results and Table 1, it is revealed that the Co-doped TiO_2 shows good rate performance compared with pure TiO_2 nanoparticles. Remarkably, among the pure and Co-doped TiO_2 nanoparticles, the 7% Co-doped TiO_2 shows the better rate performance and specific capacitance, this may be due to the 7% cobalt doping enhance the active surface, increases wettability and electronic conductivity of TiO_2 as compared to pure TiO_2, 3% Co-doped TiO_2 and 5% Co-doped TiO_2.

4. Conclusion

In summary, we have successfully synthesized the cobalt doped TiO_2 nanoparticles by a biomediated green approach using the Bengal gram bean extract. The synthesized electrode materials are explored as an anode for lithium ion battery application. The Co-doped TiO_2 anodes show better charging and discharging cycling reversibility than the pure TiO_2 anode, as cobalt doping helps to enhance the wettability with electrolyte, the formation of oxygen vacancies and the active surface on Co-doped TiO_2 anodes. Among them, the 7% Co-doped

TiO_2 anode shows highest retention capacity of 167 mAh g^{-1} (88.3%) after 100 cycles at 0.5C current density. It also shows better cycling and rate capability performance when compared to pure, 3% and 5% Co-doped TiO_2 anodes and is attributed to doping induced lowering of the band gap. Furthermore, the Co-doped TiO_2 shows higher and stable coulombic efficiency up to 100 GCD cycles indicating good reversibility. In other words, cobalt help enhancing electron transfer ability of TiO_2 nanoparticles. It is expected that this work would pave new avenues for the scientific community to develop environmentally benign metal-doped TiO_2 nanoparticles using the Bengal gram bean extract a greener and economic approach. Furthermore, metal doping is one of the best ways to enhance the electronic conductivity of TiO_2 nanoparticles and thus study is underway to understand the influence of other dopant metals and their concentration on the electrochemical performance for its application in a lithium-ion battery.

Acknowledgment

AAK is thankful to CSIR, New Delhi for the research fellowship (File No. 09/809(0013)/2012-EMR-I). The authors are thankful to the Department of Chemistry, Shivaji University Kolhapur for laboratory facilities. Financial support by Ministry of Science and Technology, R.O.C. Contract No. 105-2119-M-011-002 is acknowledged. AVG is thankful to UGC-DAE-CSR, Indore (Project Ref. No: CSR-I/CRS-48/48), UGC, New Delhi (File No. 41–370/2012 (SR)) and Shivaji University Group for Advanced Research "**SUGAR**" for the financial and characterization support

References

[1] Deng D, Kim MG, Lee JY, Cho J. Green energy storage materials: Nanostructured TiO_2 and Sn-based anodes for lithium-ion batteries. Energy Environ Sci. 2009;2(8):818-37.

[2] Song T, Paik U. TiO_2 as an active or supplemental material for lithium batteries. J Mater Chem A. 2016;4(1):14-31.

[3] Chen W, Kuang Q, Wang Q, Xie Z. Engineering a high energy surface of anatase TiO_2 crystals towards enhanced performance for energy conversion and environmental applications. RSC Adv. 2015;5(26):20396-409.

[4] Bharad PA, Sivaranjani K, Gopinath CS. A rational approach towards enhancing solar water splitting: a case study of Au-RGO/N-RGO-TiO_2. Nanoscale. 2015;7(25):11206-15.

[5] Luo C, Ren X, Dai Z, Zhang Y, Qi X, Pan C. Present Perspectives of Advanced Characterization Techniques in TiO_2-Based Photocatalysts. ACS Appl Mater Interfaces. 2017;9(28):23265-86.

[6] Zhao D, Yang C-F. Recent advances in the TiO_2/CdS nanocomposite used for photocatalytic hydrogen production and quantum-dot-sensitized solar cells. Renewable Sustainable Energy Rev. 2016;54(Supplement C):1048-59.

[7] Gong J, Sumathy K, Qiao Q, Zhou Z. Review on dye-sensitized solar cells (DSSCs): Advanced techniques and research trends. Renewable Sustainable Energy Rev. 2017;68(Part 1):234-46.

[8] Leng J, Wang Z, Li X, Guo H, Li H, Shih K, et al. Accurate construction of a hierarchical nickel–cobalt oxide multishell yolk–shell structure with large and ultrafast lithium storage capability. J Mater Chem A. 2017;5(29):14996-5001.

[9] Senthil C, Kesavan T, Bhaumik A, Yoshio M, Sasidharan M. Nitrogen Rich Carbon Coated TiO_2 Nanoparticles as Anode for High Performance Lithium-ion Battery. Electrochim Acta. 2017;255(Supplement C):417-27.

[10] Li J, Huang J, Li J, Cao L, Qi H, Cheng Y, et al. Improved Li-ion diffusion process in TiO_2/rGO anode for lithium-ion battery. J Alloys Compd. 2017;727(Supplement C):998-1005.

[11] Zhang Y, Tang Y, Li W, Chen X. Nanostructured TiO_2-Based Anode Materials for High-Performance Rechargeable Lithium-Ion Batteries. ChemNanoMat. 2016;2(8):764-75.

[12] Lee S, Eom W, Park H, Han TH. High-Temperature Stable Anatase Titanium Oxide Nanofibers for Lithium-Ion Battery Anodes. ACS Appl Mater Interfaces. 2017;9(30):25332-8.

[13] Kashale AA, Gattu KP, Ghule K, Ingole VH, Dhanayat S, Sharma R, et al. Biomediated green synthesis of TiO_2 nanoparticles for lithium ion battery application. Composites Part B. 2016;99:297-304.

[14] Zang J-L, Zhao Y-P. Silicon nanowire reinforced by single-walled carbon nanotube and its applications to anti-pulverization electrode in lithium ion battery. Compos Part B. 2012;43(1):76-82.

[15] Han H, Song T, Bae J-Y, Nazar LF, Kim H, Paik U. Nitridated TiO_2 hollow nanofibers as an anode material for high power lithium ion batteries. Energy Environ Sci. 2011;4(11):4532-6.

[16] Röser S, Lerchen A, Ibing L, Cao X, Kasnatscheew J, Glorius F, et al. Highly Effective Solid Electrolyte Interphase-Forming Electrolyte Additive Enabling High Voltage Lithium-Ion Batteries. Chem Mater. 2017;29(18):7733-9.

[17] Wang Z, Zhang F, Xing H, Gu M, An J, Zhai B, et al. Fabrication of nest-like TiO_2 hollow microspheres and its application for lithium ion batteries with high-rate performance. Electrochim Acta. 2017;243(Supplement C):112-8.

[18] Su X, Wu Q, Zhan X, Wu J, Wei S, Guo Z. Advanced titania nanostructures and composites for lithium ion battery. J Mater Sci. 2012;47(6):2519-34.

[19] Xiao L, Cao M, Mei D, Guo Y, Yao L, Qu D, et al. Preparation and electrochemical lithium storage features of TiO_2 hollow spheres. J Power Sources. 2013;238(Supplement C):197-202.

[20] Yan D, Yu C, Zhang X, Li J, Li J, Lu T, et al. Enhanced electrochemical performances of anatase TiO_2 nanotubes by synergetic doping of Ni and N for sodium-ion batteries. Electrochim Acta. 2017;254:130-9.

[21] Zheng W, Yan Z, Dai Y, Du N, Jiang X, Dai H, et al. Interpenetrated Networks between Graphitic Carbon Infilling and Ultrafine TiO_2 Nanocrystals with Patterned Macroporous Structure for High-Performance Lithium Ion Batteries. ACS Appl Mater Interfaces. 2017;9(24):20491-500.

[22] Li Y, Shen J, Li J, Liu S, Yu D, Xu R, et al. Constructing a novel strategy for carbon-doped TiO_2 multiple-phase nanocomposites toward superior electrochemical performance for lithium ion batteries and the hydrogen evolution reaction. J Mater Chem A. 2017;5(15):7055-63.

[23] Xia Y, Xiong W-S, Jiang Y, Sun W, Sang H-Q, He R-X, et al. Multi-walled carbon nanotubes induced a controllable TiO_2 morphology transformation for high-rate and long-life lithium-ion batteries. RSC Adv. 2017;7(35):21988-96.

[24] Yan Z, Hu Q, Yan G, Li H, Shih K, Yang Z, et al. Co_3O_4/Co nanoparticles enclosed graphitic carbon as anode material for high performance Li-ion batteries. Chem Eng J. 2017;321:495-501.

[25] Reddy MV, Sharma N, Adams S, Rao RP, Peterson VK, Chowdari BVR. Evaluation of undoped and M-doped TiO_2, where M = Sn, Fe, Ni/Nb, Zr, V, and Mn, for lithium-ion battery applications prepared by the molten-salt method. RSC Adv. 2015;5(37):29535-44.

[26] Chen C, Huang Y, An C, Zhang H, Wang Y, Jiao L, et al. Copper-Doped Dual Phase $Li_4Ti_5O_{12}$–TiO_2 Nanosheets as High-Rate and Long Cycle Life Anodes for High-Power Lithium-Ion Batteries. ChemSusChem. 2015;8(1):114-22.

[27] Hwang K, Sohn H, Yoon S. Mesostructured niobium-doped titanium oxide-carbon (Nb-TiO_2-C) composite as an anode for high-performance lithium-ion batteries. J Power Sources. 2018;378:225-34.

[28] Zhang W, Gong Y, Mellott NP, Liu D, Li J. Synthesis of nickel doped anatase titanate as high performance anode materials for lithium ion batteries. J Power Sources. 2015;276:39-45.

[29] Ram P, Gören A, Gonçalves R, Choudhary G, Ferdov S, Silva MM, et al. Improved electrochemical performance of rare earth doped $LiMn_{1.5-x}Ni_{0.5}RE_xO_4$ based composite cathodes for lithium-ion batteries. Compos Part B. 2018;139:55-63.

[30] Jia D, Li X, Huang J. Bio-inspired sandwich-structured carbon/silicon/titanium-oxide nanofibers composite as an anode material for lithium-ion batteries. Compos Part A Appl Sci Manuf. 2017;101:273-82.

[31] Kong H, Lv C, Yan C, Chen G. Engineering Mesoporous Single Crystals Co-Doped Fe_2O_3 for High-Performance Lithium Ion Batteries. Inorg Chem. 2017;56(14):7642-9.

[32] Zhang C, Shao D, Yu J, Zhang L, Huang X, Xu D, et al. Synthesis and electrochemical performance of cubic Co-doped $Li_4Ti_5O_{12}$ anode material for high-performance lithium-ion batteries. J Electroanal Chem. 2016;776:188-92.

[33] Thi TV, Rai AK, Gim J, Kim J. High performance of Co-doped NiO nanoparticle anode material for rechargeable lithium ion batteries. J Power Sources. 2015;292(Supplement C):23-30.

[34] Zhang W, Zhou W, Wright JH, Kim YN, Liu D, Xiao X. Mn-Doped TiO_2 Nanosheet-Based Spheres as Anode Materials for Lithium-Ion Batteries with High Performance at Elevated Temperatures. ACS Appl Mater Interfaces. 2014;6(10):7292-300.

[35] Li Q, Yin L, Li Z, Wang X, Qi Y, Ma J. Copper Doped Hollow Structured Manganese Oxide Mesocrystals with Controlled Phase Structure and Morphology as Anode Materials for Lithium Ion Battery with Improved Electrochemical Performance. ACS Appl Mater Interfaces. 2013;5(21):10975-84.

[36] Hong Z, Kang M, Chen X, Zhou K, Huang Z, Wei M. Synthesis of Mesoporous Co^{2+}-Doped TiO_2 Nanodisks Derived from Metal Organic Frameworks with Improved Sodium Storage Performance. ACS Appl Mater Interfaces. 2017;9(37):32071-9.

[37] Luo Y, Luo J, Zhou W, Qi X, Zhang H, Yu DYW, et al. Controlled synthesis of hierarchical graphene-wrapped TiO_2@Co_3O_4 coaxial nanobelt arrays for high-performance lithium storage. J Mater Chem A. 2013;1(2):273-81.

[38] Li T, Li X, Wang Z, Guo H, Li Y, Wang J. A new design concept for preparing nickel-foam-supported metal oxide microspheres with superior electrochemical properties. J Mater Chem A. 2017;5(26):13469-74.

[39] Kashale AA, Ghule KA, Gattu KP, Ingole VH, Dhanayat SS, Sharma R, et al. Annealing atmosphere dependant properties of biosynthesized TiO_2 anode for lithium ion battery application. J Mater Sci Mater Electron. 2017;28(2):1472-9.

[40] Lorite I, Romero JJ, Fernández JF. Effects of the agglomeration state on the Raman properties of Co_3O_4 nanoparticles. J Raman Spectrosc. 2012;43(10):1443-8.

[41] Fan D, Weirong Z, Zhongbiao W. Characterization and photocatalytic activities of C, N and S co-doped TiO_2 with 1D nanostructure prepared by the nano-confinement effect. Nanotechnology. 2008;19(36):365607.

[42] Delekar SD, Dhodamani AG, More KV, Dongale TD, Kamat RK, Acquah SFA, et al. Structural and Optical Properties of Nanocrystalline TiO_2 with Multiwalled Carbon Nanotubes and Its Photovoltaic Studies Using Ru(II) Sensitizers. ACS Omega. 2018;3(3):2743-56.

[43] Lubke M, Shin J, Marchand P, Brett D, Shearing P, Liu Z, et al. Highly pseudocapacitive Nb-doped TiO_2 high power anodes for lithium-ion batteries. J Mater Chem A. 2015;3(45):22908-14.

[44] Hao B, Yan Y, Wang X, Chen G. Synthesis of Anatase TiO_2 Nanosheets with Enhanced Pseudocapacitive Contribution for Fast Lithium Storage. ACS Appl Mater Interfaces. 2013;5(13):6285-91.

[45] Wang J, Zhou Y, Hu Y, O'Hayre R, Shao Z. Porous nanocrystalline TiO_2 with high lithium-ion insertion performance. J Mater Sci. 2013;48(6):2733-42.

[46] Yadav HM, Otari SV, Koli VB, Mali SS, Hong CK, Pawar SH, et al. Preparation and characterization of copper-doped anatase TiO_2 nanoparticles with visible light photocatalytic antibacterial activity. J Photochem Photobiol, A. 2014;280:32-8.

[47] Liu Y, Xiao R, Fang Y, Zhang P. Three-Dimensional Oxygen-Deficient $Li_4Ti_5O_{12}$ Nanospheres as High-Performance Anode for Lithium Ion Batteries. Electrochim Acta. 2016;211:1041-7.

[48] Xu W, Cui X, Xie Z, Dietrich G, Wang Y. Integrated Co_3O_4/TiO_2 Composite Hollow Polyhedrons Prepared via Cation-exchange Metal-Organic Framework for Superior Lithium-ion Batteries. Electrochim Acta. 2016;222:1021-8.

[49] Sudant G, Baudrin E, Larcher D, Tarascon J-M. Electrochemical lithium reactivity with nanotextured anatase-type TiO_2. J Mater Chem A. 2005;15(12):1263-9.

[50] Kim J, Cho J. Rate Characteristics of Anatase TiO_2 Nanotubes and Nanorods for Lithium Battery Anode Materials at Room Temperature. J Electrochem Soc. 2007;154(6):A542-A6.

[51] Suresh Kumar P, Aravindan V, Sundaramurthy J, Thavasi V, Mhaisalkar SG, Ramakrishna S, et al. High performance lithium-ion cells using one dimensional electrospun TiO_2 nanofibers with spinel cathode. RSC Adv. 2012;2(21):7983-7.

Table and Table caption

Table 1. Specific capacity values at a different rate obtained for pure TiO_2 and Co-doped TiO_2 nanoparticles based anode.

Current Density	**Specific Capacitance of Electrodes (mAh g^{-1})**			
	Pure TiO_2 (mAh g^{-1})	**3% Co-doped TiO_2 (mAh g^{-1})**	**5% Co-doped TiO_2 (mAh g^{-1})**	**7% Co-doped TiO_2 (mAh g^{-1})**
0.1 C	183	170	192	221
0.2 C	125	146	152	188
0.5 C	85	105	119	157
1 C	71	91	84	122
2 C	55	70	61	93
5 C	38	32	39	70
0.1 C	127	148	176	202

Figure and Figure Captions:

Figure 1 Representative X-ray diffraction patterns of biosynthesized (a) pure TiO_2 (b) 3% Co -TiO_2 (c) 5% Co -TiO_2 and (d) 7% Co -TiO_2.

Figure 2 Representative Raman Spectra of biosynthesized (a) pure TiO_2 (b) 3% Co-TiO_2 (c) 5% Co-TiO_2 and (d) 7% Co-TiO_2

Figure 3 Representative UV-Vis diffuse reflectance spectra of biosynthesized (a) pure TiO_2 (b) 3% Co -TiO_2 (c) 5% Co -TiO_2 and (d) 7% Co -TiO_2

Figure 4 Representative SEM images of biosynthesized (a) pure TiO_2 (b) 3% Co -TiO_2 (c) 5% Co -TiO_2 and (d) 7% Co -TiO_2.

Figure 5 Representative EDAX spectra of biosynthesized (a) pure TiO_2 and (b) 5% Co -TiO_2

Figure 6 Representative TEM images of biosynthesized (a-b) pure TiO_2 (c-d) 5% Co -TiO_2 and represent histograms of (e) pure -TiO_2 and (f) 5% Co -TiO_2

Figure7 (a) Cyclic voltammetry curves at scan rate of 0.2 mV S^{-1} (b) Charge-discharge profiles cycled at a current density of 0.1 C; (c) cycle performance up to 100 cycled at a current density of 0.5 C and (d) rate performance at various C-rate of Pure TiO_2, 3% Co-doped TiO_2, 5% Co-doped TiO_2 and 7% Co-doped TiO_2.

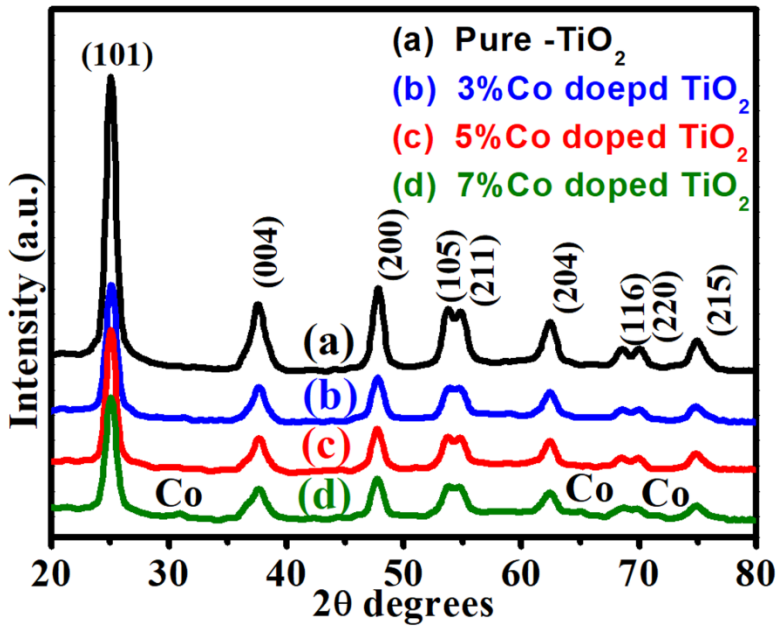

Figure 1 Kashale et. al.

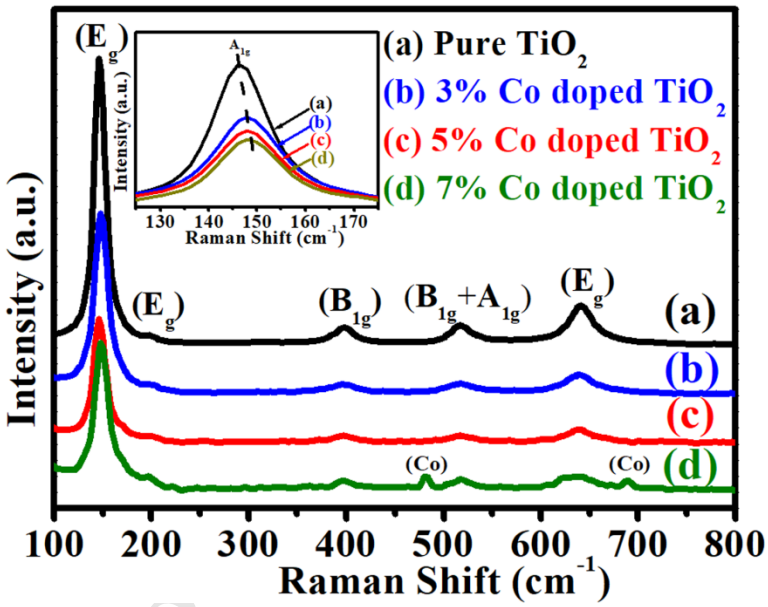

Figure 2 Kashale et. al.

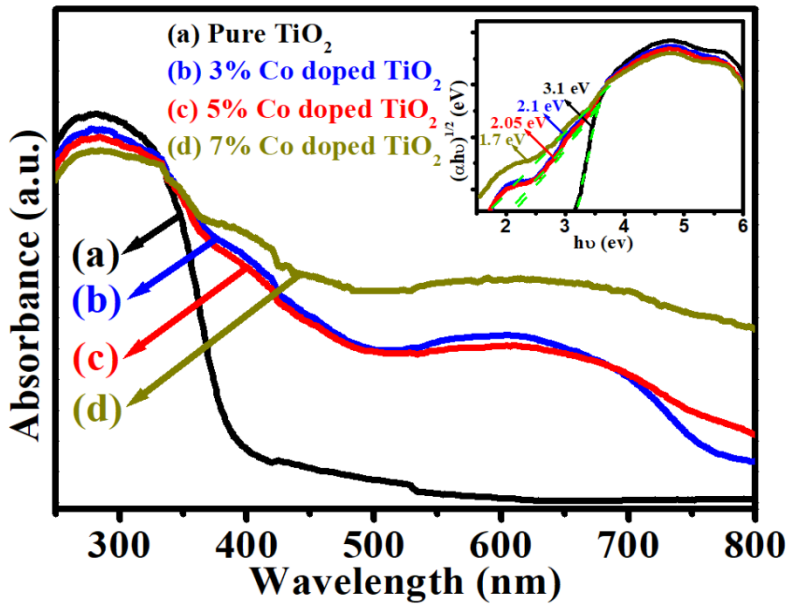

Figure 3 Kashale et. al.

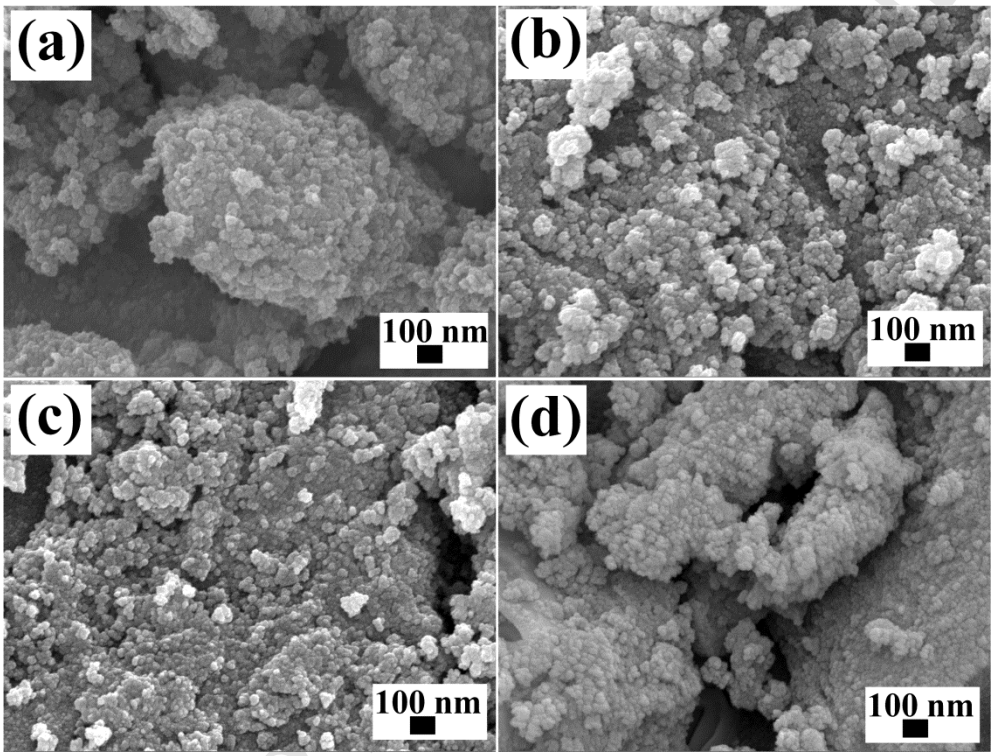

Figure 4 Kashale et. al.

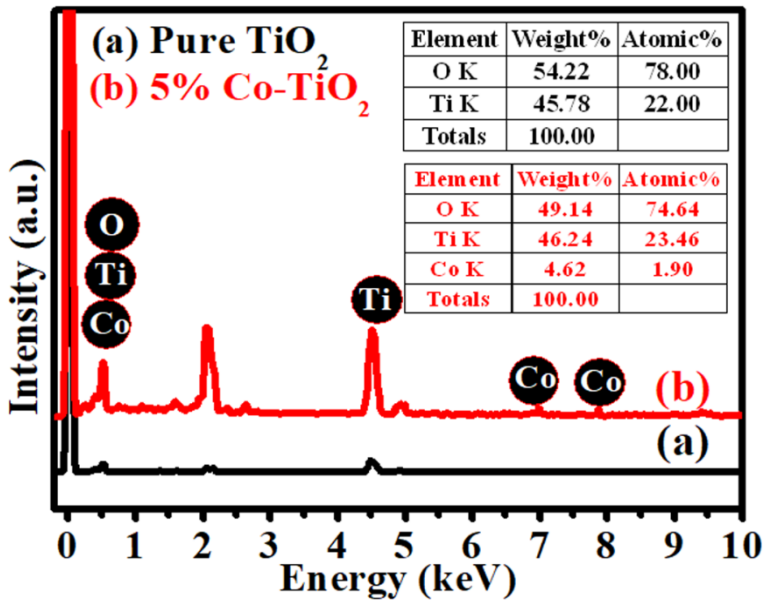

Figure 5 Kashale et. al.

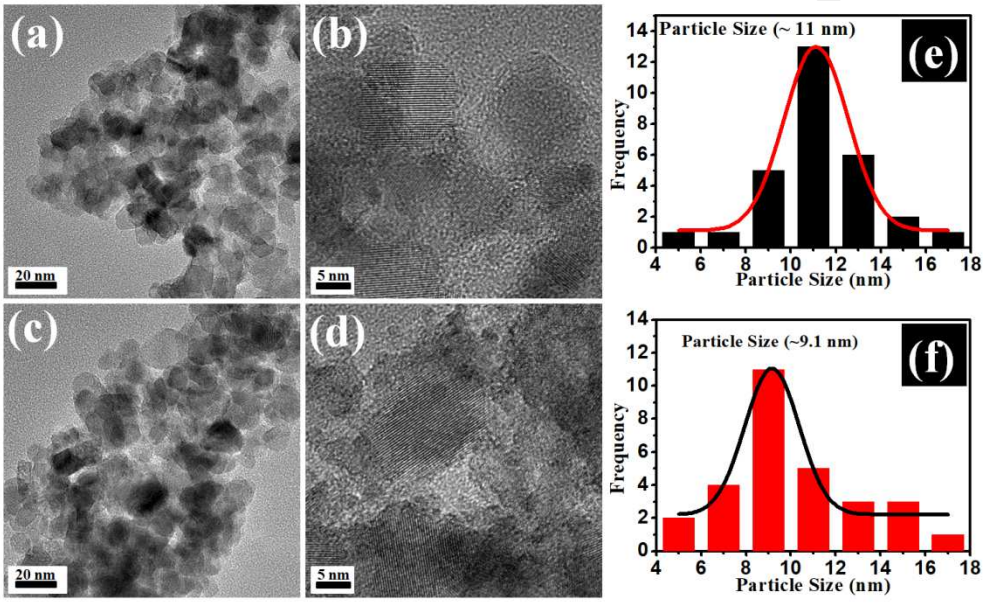

Figure 6 Kashale et. al.

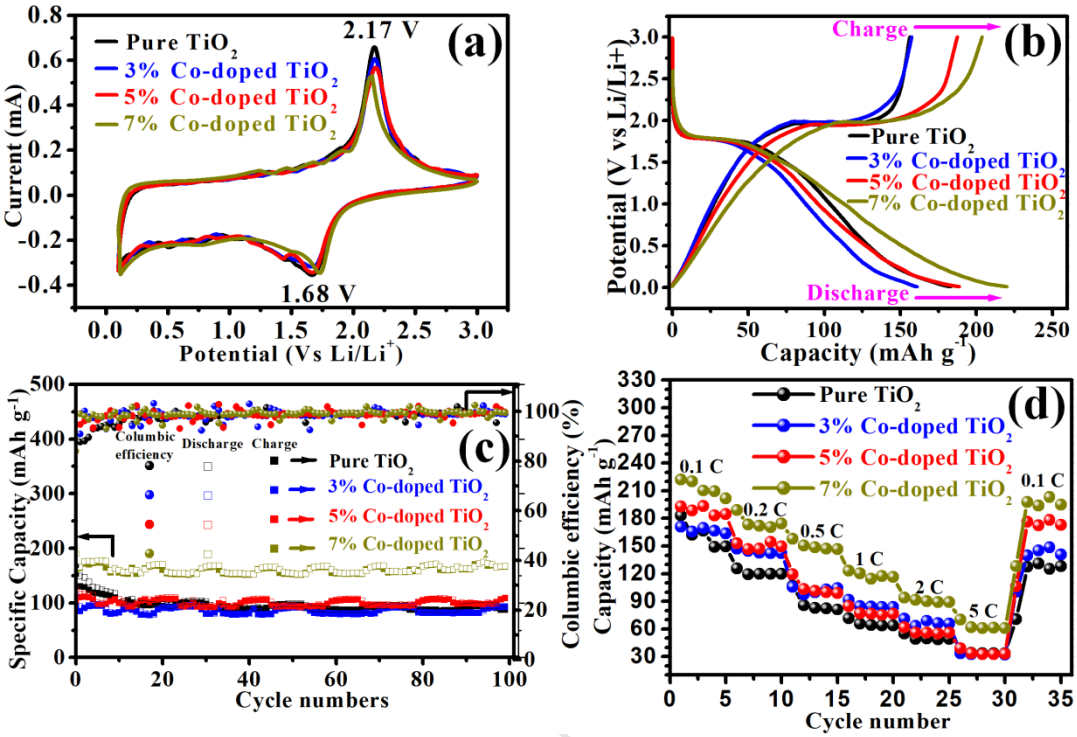

Figure 7 Kashale et. al.

Highlights

- Simple biomediated approach used for synthesis of pure TiO_2 and Co-doped TiO_2 NPs.
- Pure TiO_2 and Co-doped TiO_2 NPs are explored as anode material in lithium ion battery.
- Co doping enhances the electronic/ionic conductivity of TiO_2.
- Co doping reduces the charge-discharge irreversible capacity when compared to pure TiO_2.
- 7% Co-doped TiO_2 NPs show better specific capacitance (189 mAh g^{-1}), rate capability and stability with 88.3 % retention even after 100 GCD cycles.
- Coulombic efficiency study of Co-doped TiO_2 shows good reversibility upto 100 GCD cycles.